The Astrophysical Journal, 843:10 (7pp), 2017 July 1 https://doi.org/10.3847/1538-4357/aa72e7

New Evidence for a Coronal Mass Ejection-driven High Frequency Type II Burst near the Sun

Anshu Kumari[1], R. Ramesh[1], C. Kathiravan[1], and N. Gopalswamy[2]
[1] Indian Institute of Astrophysics, 2nd Block, Koramangala, Bangalore—560 034, Karnataka, India; anshu@iiap.res.in
[2] Code 671, Solar Physics Laboratory, NASA/GSFC, Greenbelt, MD, USA
Received 2017 February 17; revised 2017 April 27; accepted 2017 April 30; published 2017 June 26

Abstract

We report observations of the high frequency type II radio burst (≈430–30 MHz) that occurred in the solar corona on 2015 November 4. The drift rate of the burst, estimated close to the start frequency of its fundamental component (≈215 MHz), is unusually high (≈2 MHz s^{-1}). Our analysis shows that the estimated speed of the magnetohydrodynamic shock driver of the burst varies with time. The peak speed and acceleration are very large, ≈2450 km s^{-1} and ≈17 km s^{-2}, respectively. There is spatio-temporal correlation between the type II burst and the associated coronal mass ejection (CME) in the whitelight and extreme-ultraviolet images. The time profile of the shock speed and the light curve of the associated soft X-ray flare correlate well. These results indicate that in the present case, (i) the magnetohydrodynamic shock responsible for the high frequency coronal type II burst is driven by the CME and (ii) the time profile of the type II burst shock speed represents the near-Sun kinematics of the CME.

Key words: Sun: activity – Sun: corona – Sun: coronal mass ejections (CMEs) – Sun: flares – Sun: magnetic fields – Sun: radio radiation

1. Introduction

Type II solar radio bursts are considered to originate from plasma waves excited by magnetohydrodynamic (MHD) shocks and converted into radio waves at the local plasma frequency and/or its harmonics. They are the direct diagnostic of MHD shocks in the solar atmosphere. The burst is recognized in radio spectral observations, where the intensity is plotted in the time–frequency plane, as a drift toward lower frequencies. This drift results from the decrease of the electron density with distance from the surface of the Sun. Both flares and coronal mass ejections (CMEs) are potential drivers of MHD shocks in the solar atmosphere (see Nindos et al. 2008 for a review on the topic). It is widely accepted now that the low frequency ($\lesssim$14 MHz) type II bursts observed in the outer corona ($r > 3\ R_\odot$, where r is the heliocentric distance) and the interplanetary medium are due to MHD shocks piston-driven by the associated CMEs (see Gopalswamy 2006 for a review on the topic). One of the main reasons for this is that simultaneous observations of CMEs in whitelight are available for almost all the bursts in the corresponding distance where the bursts are observed. Even in the case of coronal type II bursts with start frequencies <150 MHz, spatio-temporal association with CMEs has been extensively reported (see for example Cliver et al. 1999, 2004; Claßsen & Aurass 2002; Mancuso & Raymond 2004; Cho et al. 2005, 2008; Liu et al. 2009; Ramesh et al. 2010b, 2012a; Ma et al. 2011; Hariharan et al. 2014, 2015; Zucca et al. 2014). The high frequency coronal type II bursts (start frequencies >150 MHz) however seem to be an exception. The bursts are attributed to MHD shocks driven by flare blast waves (Vršnak et al. 1995; Shanmugaraju et al. 2009; Magdalenić et al. 2012). But EUV observations show CME/shock formation associated with type II radio bursts with start frequency ≈150 MHz (Gopalswamy et al. 2012). Therefore, it is likely that the above discrepancy could be due to the fact that the high frequency type II bursts originate close to the Sun (i.e., over $r \lesssim 1.5\ R_\odot$), where whitelight observations of CMEs and their kinematics are limited at present. In this situation, we report for the first time the shock speed profile of a CME-associated high frequency coronal type II burst and its correlation with the light curve of the associated soft X-ray flare. This study shows that high frequency type II bursts and the associated X-ray flare observations with high temporal resolution help us to understand the kinematics of the associated CMEs close to the Sun.

2. Observations

The radio imaging and spectral observations were carried out with the Gauribidanur RAdioheliograPH (GRAPH; Ramesh et al. 1998, 1999a, 2006b) at 80 MHz, and the Gauribidanur RAdio SpectroPolarimeter (GRASP; Kishore et al. 2015) in the frequency range 440–40 MHz, respectively. Both the above instruments are operated in the Gauribidanur observatory[3] (Ramesh 2011a). The angular resolution of the GRAPH is ≈5′ × 7′ (R.A. × decl.) at the above frequency. The integration time is ≈250 ms. The half-power width of the response pattern of GRASP is ≈90° × 60° (R.A. × decl.) and is nearly independent of frequency. The primary receiving element used in GRASP is a Crossed Log-Periodic Dipole (Sasikumar Raja et al. 2013a). The integration time is ≈250 ms, and the observing bandwidth is ≈300 KHz at each frequency. The antenna and the receiver systems were calibrated by carrying out observations in the direction of the Galactic center as described in Kishore et al. (2015). We used images obtained in whitelight with the Large Angle and Spectrometric Coronagraph (LASCO; Brueckner et al. 1995) on board the *Solar and Heliospheric Observatory* (*SOHO*) for information on the CMEs, and in 171 Å/211 Å with the Atmospheric Imaging Assembly (AIA; Lemen et al. 2012) on board the *Solar Dynamics Observatory* (*SDO*) to identify the source region of the CMEs and their counterparts closer to the Sun.

[3] http://www.iiap.res.in/centers/radio

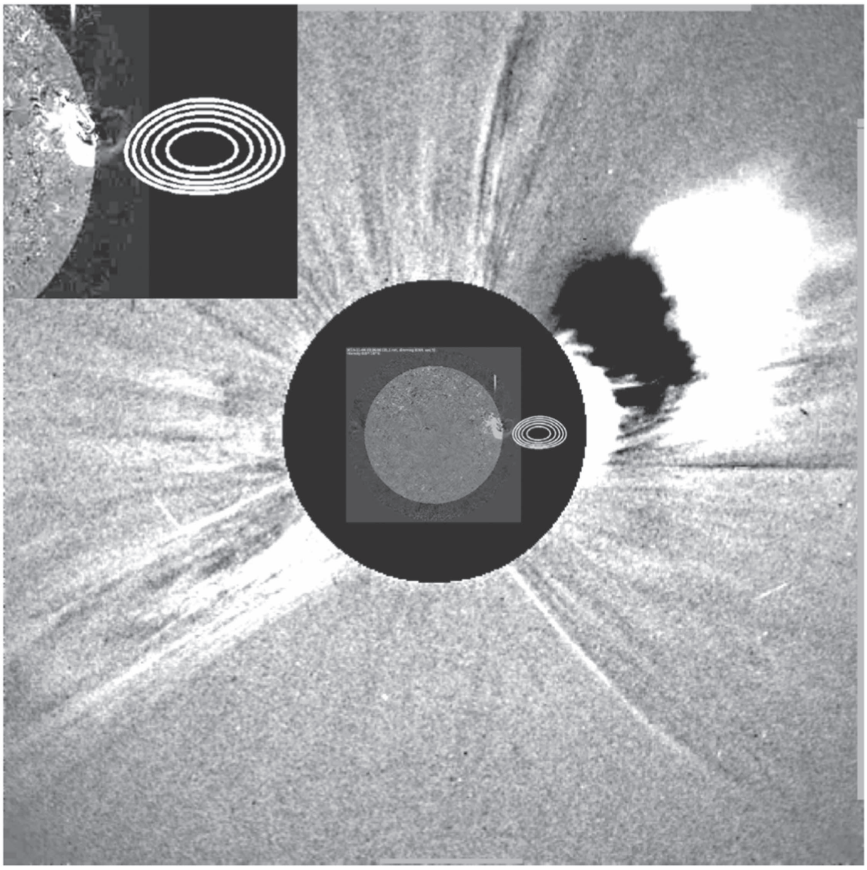

Figure 1. Composite of the 80 MHz radioheliogram of the type II burst observed on 2015 November 4 at 03:31 UT with GRAPH, the associated *SOHO*/LASCO-C2 difference image obtained at ≈04:00 UT, and the *SDO*/AIA 211 Å image obtained at ≈03:26 UT. Solar north is straight up and east is to the left. The "black" circle indicates the occulting disk of the coronagraph. Its radius is ≈2.2 $R_{\odot}$. The bright emission emerging above the coronagraph occulter on its west corresponds to the CME mentioned in the text. The other dark and bright features located farther above in nearly the same P.A. range correspond to an earlier CME that was first observed in the *SOHO*/LASCO-C2 FOV at ≈02:12 UT. The intense discrete radio source (shown in white contours) at $r \approx 1.5\ R_{\odot}$ is the type II burst mentioned in the text. Its peak brightness temperature (T_b) is $\approx 2.2 \times 10^8$ K. The contours shown (inner to outermost) are at 97.5%, 95%, 92.5%, 90%, and 87.5% of the peak T_b. The contour interval is 5.5×10^6 K. The inset is a close-up view of the activity in AR1 2445 observed with *SDO*/AIA 211 Å and the location of the radio burst. The CME can be noticed as a faint loop-like structure above the limb. Its LE is located at ≈1.1 $R_{\odot}$.

Figure 1 shows the composite of the type II burst observed with GRAPH on 2015 November 4 at 03:31 UT, the *SOHO*/LASCO-C2 running difference image of the associated CME around ≈04:00 UT—the epoch at which it was first noticed in the field of view (FOV) of the coronagraph, and the *SDO*/AIA 211 Å image obtained at ≈03:26 UT. The central position angle (P.A., measured counterclockwise from the solar north) of the CME is ≈278°, and its angular width is ≈64°. Its leading edge (LE) is located around $\approx 2.8 \pm 0.4\ R_{\odot}$.[4] The position of the centroid of the type II burst is $\approx 1.5 \pm 0.2\ R_{\odot}$. Any possible error in the position of the burst due to propagation effects such as scattering by density inhomogeneities in the solar corona and/or refraction in the Earth's ionosphere is expected to be within the above error limit (Stewart & McLean 1982; Ramesh et al. 1999b, 2006a, 2012b; Kathiravan et al. 2011; Mercier et al. 2015; Mugundhan et al. 2016). The fact that the Sun is presently going through a period of extended minimum (during which the observations reported in this work were carried out) also indicates that scattering will be less (Sasikumar Raja et al. 2016). The GRAPH observations at 80 MHz were ≈29 minutes before the CME appeared in the *SOHO*/LASCO-C2 FOV. Figure 2 shows the GRASP observations of the dynamic spectrum of the aforementioned type II burst in both Stokes *I* and *V*. The onset frequency is ≈430 MHz at ≈03:25:05 UT. The fundamental and harmonic emission bands can be clearly noticed. Their spectral widths are consistent with those of similar high frequency type II bursts reported in the literature (see, for example, Zimovets et al. 2012; Cho et al. 2013). The burst was also present in the Gauribidanur LOw-frequency Solar Spectrometer (GLOSS; Ebenezer et al. 2007; Kishore et al. 2014) observations carried out over the frequency range 85–35 MHz and the e-CALLISTO observations elsewhere during the same epoch (Monstein et al. 2007; Benz et al. 2009). This helped to independently establish the spectral class of the burst. An inspection of the observations on 2015 November 4 with the *Wind*/WAVES instrument indicates that the above burst was limited to frequencies >14 MHz, i.e., it did not extend into the interplanetary medium.[5] The low frequency cutoff must have probably been somewhere between 35 and 14 MHz. An inspection of the GLOSS dynamic spectrum[6] indicates that the GRAPH observations in Figure 1 at 80 MHz corresponds to the harmonic component of the type II burst. These strengthen our above assumption regarding the source

[4] https://cdaw.gsfc.nasa.gov

[5] http://solar-radio.gsfc.nasa.gov/index.html

[6] http://www.iiap.res.in/files/solarradioimages/gbd/GLOSS_20151104.jpg

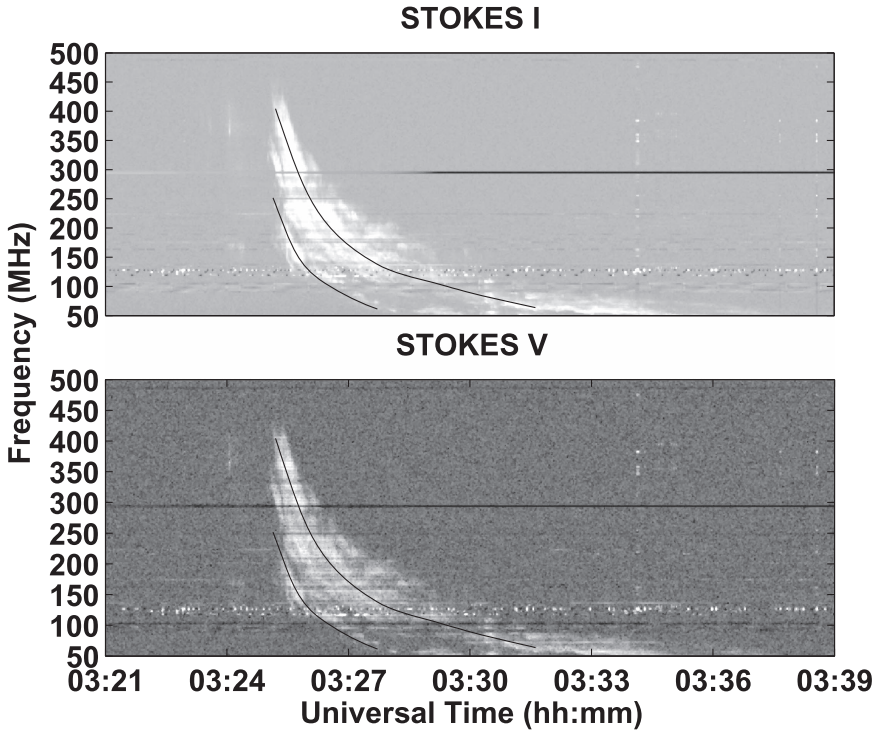

Figure 2. GRASP observations of the Stokes-*I* (upper panel) and Stokes-*V* (lower panel) dynamic spectra of the type II burst of 2015 November 4 in Figure 1. The curved black colored lines superposed on the bright, drifting emission features indicate the fundamental (lower black line) and harmonic (upper black line) emission components of the burst. The horizontal features in the spectra close to 300 and 100 MHz are due to local radio frequency interference (RFI).

position since the effects of scattering on the position of the harmonic component of a solar radio burst is expected to be minimal compared to the fundamental component (Riddle 1974; Robinson 1983). The X-Ray Sensor (XRS) on board the *Geostationary Operational Environmental Satellite* (*GOES-15*) recorded an M1.9 class soft X-ray flare from AR 12445 located at N14W64 on the Sun[7] during the interval ≈03:20–03:29 UT. The flare maximum was at ≈03:25 UT. There was also a 1N class Hα flare during the interval ≈03:23–03:34 UT, with maximum at ≈03:25 UT.[8] We independently verified this using observations with the Hα telescope in the Kodaikanal Observatory (Ravindra et al. 2016). A comparison of the above timings indicate that the type II burst occurred almost at the same time as the flare maximum. An inspection of the successive *SDO*/AIA images revealed that the above CME was accompanied by an extreme-ultraviolet (EUV) wave from the associated active region (Thompson et al. 1998).

3. Analysis and Results

As mentioned earlier, the 80 MHz type II burst in Figure 1 corresponds to the harmonic component and is located at ≈1.5 $R_\odot$. The corresponding deprojected location is ≈1.7 $R_\odot$. This agrees reasonably with the location of the 40 MHz plasma layer (fundamental component of the burst) estimated using the relationship between the starting frequency (f) of the type II bursts and r corresponding to the LE of the associated CME, i.e., $f(r) = 307.87r^{-3.78} - 0.14$ derived by Gopalswamy et al. (2013b). We converted the above power law to a "model" (hereinafter referred to as the Gopalswamy model) for the electron density distribution ($N_e(r)$) using the equality $f(r) = 9 \times 10^{-3}\sqrt{N_e(r)}$ (where $f(r)$ and $N_e(r)$ are in units of MHz and cm^{-3}, respectively) and estimated the speed of the MHD shock associated with the type II burst in Figure 2. Note that we used the above relationship since it was obtained from a statistical study of type II bursts and the associated CMEs. The assumptions were very minimal, and the list included events with high starting frequencies as in the present case. The associated CMEs were "limb" events. So, the projection effects are expected to be less. Further, both the CME LE and the EUV wave diameter methods used by the authors (to infer the CME height at the time of type II burst onset) gave nearly identical results for the events where it was possible for them to use both methods. Finally, the $r^{-7.56}$ density variation in the above model takes care of possible "clearing" of the corona by the preceding CME as in the present case (see caption for Figure 1). In this regard, we would like to point out that Ramesh & Sastry (2000) had estimated that the density varies as r^{-10} in the region of the corona where a CME-induced depletion was observed. Note that according to the conventional density models (derived mostly using whitelight observations carried out during total solar eclipses), the density varies uniformly as $\propto r^{-6}$ in the "middle" corona, i.e., $1.1 \lesssim r \lesssim 3.0\ R_\odot$.

Figure 3 shows the height–time (h–t) details of the CME LE in *SOHO*/LASCO-C2 observations, EUV wavefront LE in the *SDO*/AIA 171 Å images, and the location of the type II burst in observations with GRAPH at 80 MHz and GRASP at select frequencies. The EUV and radio measurements are in the distance range $r \approx 1$–$2\ R_\odot$. Initially, both the EUV wavefront and the type II burst exhibit acceleration, and there is also good consistency between their h–t measurements. But the EUV wavefront slows down after a while. The type II burst shows continued acceleration for some more time (see Figure 4). Later, it also slows down, and its h–t measurements matches

[7] www.lmsal.com/solarsoft/latest_events
[8] ftp://ftp.swpc.noaa.gov/pub/warehouse

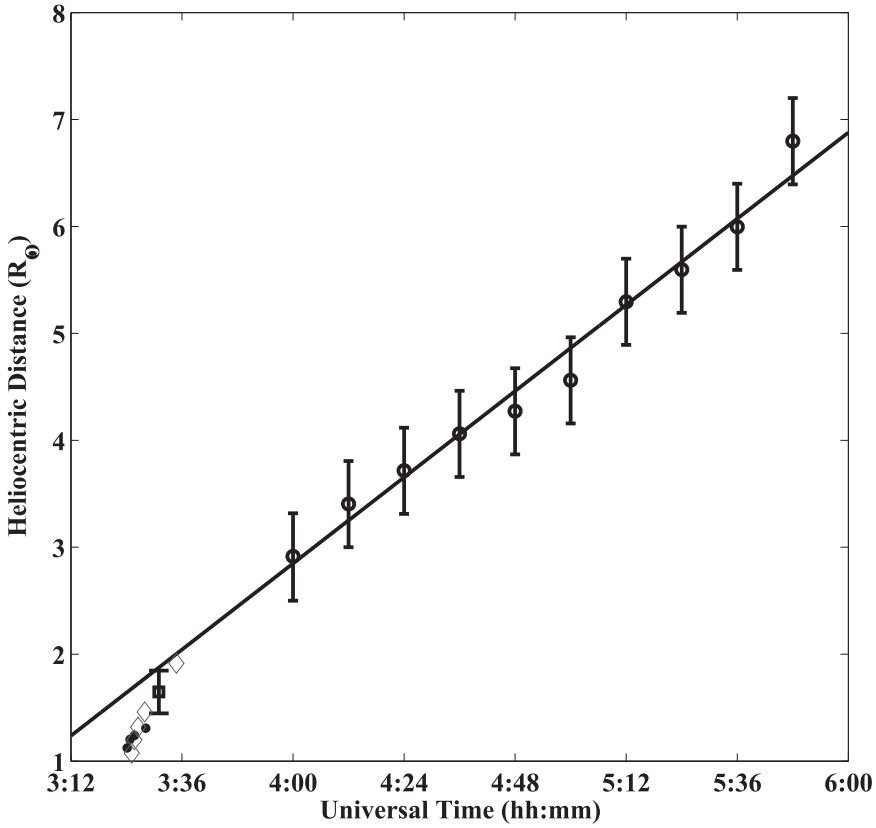

Figure 3. Height–time plot of the CME LE (indicated by the circles) observed with the *SOHO*/LASCO-C2 coronagraph, LE of the EUV wavefront (indicated by the dots) observed with *SDO*/AIA 171 Å, and the type II burst observed with GRAPH at 80 MHz (indicated by the square) and with GRASP at select frequencies (430, 310, 215, 150, 50 MHz—indicated by the diamonds). Note that all of the aforementioned frequencies correspond to the harmonic component of the type II burst.

with the linear extrapolation (in the Sunward direction) of similar measurements of the CME LE (over the range ≈3–7 $R_\odot$). This indicates a close association between the type II burst and the CME LE.

Since the duration of the burst is long in the present case (≈10 minutes in the frequency range ≈430–50 MHz), we estimated the speed of the associated shock at different time intervals. The start and end frequencies of the burst were different in each estimation. The results are shown in Figure 4 along with the X-ray light curve obtained with *GOES-15*/XRS in the 1.6–12.4 keV (1–8 Å) energy band and the time profile of the EUV 171 Å wavefront speed. We find that the onset of the type II burst at ≈03:25:05 UT is close to the time (≈03:24:35 UT) when the speed of the EUV wavefront was the maximum (≈1893 km s^{-1}). There is also a good agreement between the latter and the initial shock speed of the type II burst (≈1958 km s^{-1}). The above consistency in the speeds and the initial agreement between their *h*–*t* measurements (see Figure 3) indicate that the type II burst and the EUV wave are both driven by the same CME (Patsourakos & Vourlidas 2012; Liu & Ofman 2014). But the observational evidences that the onset of the EUV wave (≈03:24:10 UT) is about one minute earlier to the onset of the type II burst and the EUV wavefront starts decelerating earlier (≈03:24:35 UT) compared to the type II burst (≈03:25:30 UT) suggest otherwise (see, for example, Kumar et al. 2016). This needs to be verified statistically.

Figure 4 indicates that the type II burst shock speed increased from ≈1958 km s^{-1} to ≈2441 km s^{-1} during the interval ≈03:25:05–03:25:30 UT. The corresponding acceleration is ≈17 km s^{-2}. Such a large acceleration, though unreported, is likely (Vršnak & Cliver 2008). Cho et al. (2013) had reported a similar high frequency type II burst associated with a CME event, but from near the center of the solar disk, where the latter exhibited a strong acceleration (≈8 km s^{-2}) for a very short time interval of ≈1 minute as in the present case. Note that the drift rate of the burst, estimated close to ≈215 MHz (the start frequency of the fundamental component; see Figure 2) is ≈2 MHz s^{-1}. The shock speed decreased to ≈1910 km s^{-1} at ≈03:27 UT. The deceleration during this interval is ≈−6 km s^{-2}. The deceleration beyond ≈03:27 UT is ≈−2 km s^{-2}. The speed of the shock close to ≈03:33 UT is ≈1125 km s^{-1}. We estimated the probable location of the type II burst at 03:25:34 UT (i.e., when the shock speed was at maximum) based on its deprojected location of ≈1.7 ± 0.2 $R_\odot$ at 03:31 UT and the kinematics of the associated MHD shock during the interval between the above two epochs. The calculations indicate that the burst should have been located at $\lesssim$1.12 $R_\odot$. This is reasonably consistent with the location of the CME LE in the *SDO*/AIA 211 Å image at ≈03:26 UT (see Figure 1). This implies that the peak acceleration of the CME in the present case was over by the time it reached $r \approx 1.1\ R_\odot$. This agrees well with the reports that the CMEs reach their peak acceleration at $r \lesssim 1.5\ R_\odot$ (Bein et al. 2011), and the MHD shock associated with high frequency ($\gtrsim$200 MHz) type II bursts occurs at $r < 1.2\ R_\odot$ (Gopalswamy et al. 2013b). Note that the drift rate of the burst, estimated close to ≈215 MHz (the start frequency of the fundamental component; see Figure 2), is ≈2 MHz s^{-1}. Unusually high drift rates like this, which are probably indicative of a fast shock, seem to be typical of high frequency

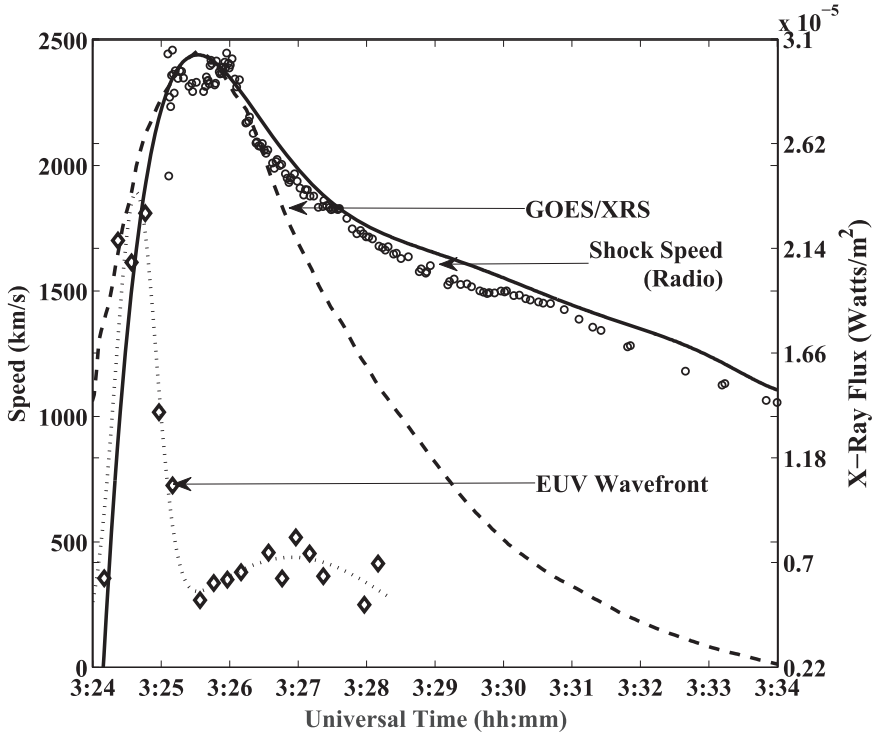

Figure 4. Time profile of the MHD shock speed (indicated by the circles) corresponding to the type II burst in Figure 2, time profile of the speed of the LE of the *SDO*/AIA 171 Å EUV wavefront (indicated by the diamonds), and the *GOES-15*/XRS light curve of the associated X-ray flare (indicated by the dashed line) obtained with a temporal resolution of ≈2 s. The thick line is the fit to the shock speed estimates, and the dotted line is the fit to the EUV measurements.

type II bursts (see, for example, Mann et al. 1996; Pohjolainen et al. 2008; Zimovets et al. 2012).

There is a good correspondence between the time profile of the type II burst shock speed and the X-ray light curve of the flare (see Figure 4). The cross-correlation coefficient between the shock speed and the X-ray flux is ≈0.86 (see Figure 5). Furthermore, the maximum in both cases occurred at almost the same time (≈03:25:30 UT). Variation of the CME speed in the low corona mimicking the X-ray light curve has been reported in the literature (Zhang et al. 2001; Temmer et al. 2008; Gopalswamy et al. 2009; Temmer et al. 2010). In this work, we find an independent confirmation of this result using the speed variation of the CME-driven shock from radio observations alone for the first time. Considering that there is also good spatio-temporal correlation between the CME LE and the type II burst in the present case (see Figure 3 and the previous paragraph), the time profile of the shock speed of the latter can be considered to represent the near-Sun kinematics of the CME.

The fundamental component (f_p) of the start frequency of the type II burst in Figure 2 is ≈215 MHz as mentioned earlier. This is ≈2× higher than the average value of ≈100 MHz (fundamental component) for similar "limb" type II bursts (Gopalswamy et al. 2005). Therefore, it is likely that the present CME occurred in a strong field region with fast magnetic reconnection (see, for example, Lin et al. 2006). An estimate of the coronal magnetic field strength B using the empirical relation $B = f_p \times dcp/2.8a(\theta)$ for harmonic plasma emission (Dulk & Suzuki 1980) indicates that $B \approx 3$ G at a typical frequency like 80 MHz ($f_p = 40$ MHz) in the present case. Note that $a(\theta)$ is a slowly varying function of the angle θ between the line of sight and direction of the magnetic field in the source region. Its value is $\gtrsim 1$ for source regions near the solar limb as in Figure 1 (Dulk & McLean 1978; Ramesh et al. 2010a). We assumed $a(\theta) = 1$ for our calculations. dcp $(=V/I)$ is the degree of circular polarization. Its estimated value from the Stokes I and V observations of the type II burst in Figure 2 is ≈0.22 at 80 MHz. Interestingly, the above value of B is equal to that obtained independently using the formula for Alfvén speed, i.e., $v_A = B/\sqrt{4\pi M N_e}$, where $M = 1.9 \times 10^{-24}$ g is the mass ascribed to each electron in the plasma (includes 10% He). We assumed $v_A \approx 1400$ km s^{-1}, i.e., the MHD shock speed at 03:31 UT (see Figure 4) when the harmonic component of the type II burst was observed with GRAPH at 80 MHz (see Figure 1). $N_e = 2 \times 10^7$ cm^{-3} is the electron density corresponding to $f_p = 40$ MHz. The above estimates of B are about 2× higher than those reported in the literature from type II burst observations around $r \approx 1.5\ R_\odot$ (see, for example, Gopalswamy et al. 2012; Kishore et al. 2016), and 5× higher than the active region field strength when there are no type II bursts (see, for example, Ramesh et al. 2011b). This is consistent with our above remark that the CME possibly occurred in a strong field region. The ≈2× higher start frequency of the type II burst compared to the average value reported in the literature is in support of the above argument since $B \propto f_p$. Earlier reports also indicate that $B \approx 3$ G at $r \approx 1.5\ R_\odot$ during a CME or transient radio burst activity is not uncommon (Vršnak et al. 2002; Ramesh et al. 2003, 2013; Sasikumar Raja & Ramesh 2013b).

CMEs associated with solar energetic particle (SEP) events and ground-level enhancement are known to have speeds >2000 km s^{-1}, and acceleration >2 km s^{-2}. The shock formation heights in such events is typically 1.5 $R_\odot$ (Gopalswamy et al. 2013a). Surprisingly, there is no SEP event above the background level in the *GOES* > 10 MeV channel in the present case. The type II burst implies acceleration of ∼10 keV

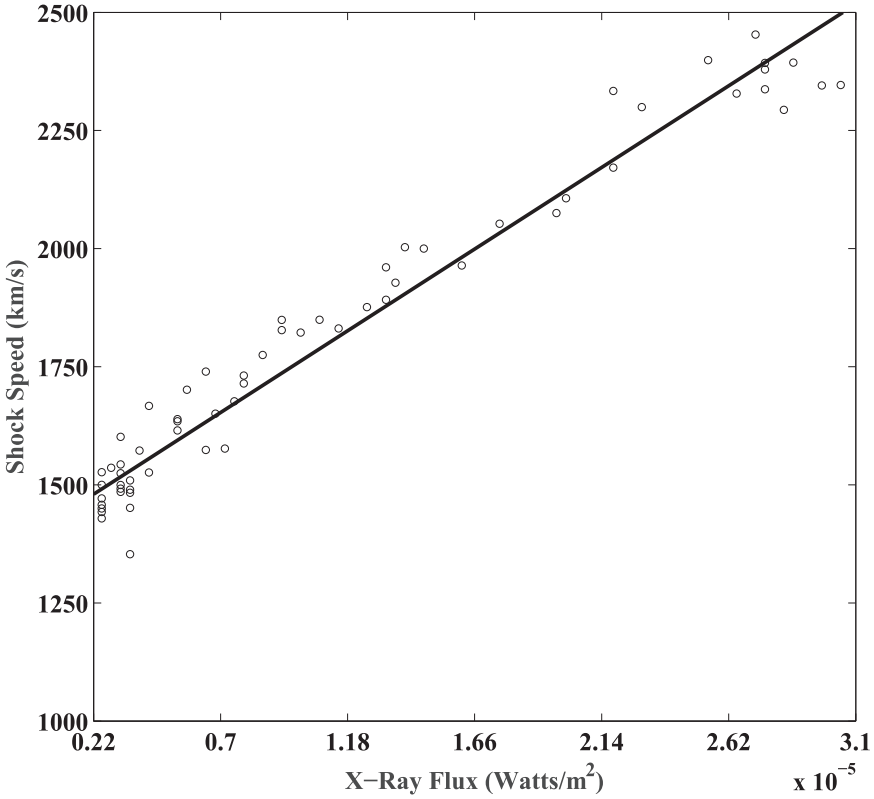

Figure 5. Cross-correlation between the type II burst shock speed and the X-ray flare flux in Figure 4. The correlation coefficient is ≈0.86.

electrons by the shock. However, there seems to be not enough time for the shock to accelerate ions to sufficiently high energies because the shock had >2000 km s^{-1} speed only for a couple of minutes (see Figure 4). Furthermore, v_A in the source region is high, so the Mach number is low even though the shock speed is high.

4. Summary

We have reported a high frequency type II burst with an unusually high drift rate (≈2 MHz s^{-1}). The estimated speed of the MHD shock driver of the burst varies with time. The peak speed and acceleration are considerably large, ≈2500 km s^{-1} and ≈17 km s^{-2}, respectively. The time profile of the shock speed derived from radio observations correlates well with the light curve of the associated soft X-ray flare. Since there is also spatio-temporal association between the type II burst and the associated CME, the results indicate that (i) the high frequency coronal type II burst is due to MHD shock driven by the CME and (ii) the shock speed profile of the type II burst represents the near-Sun kinematics of the CME.

We thank the staff of the Gauribidanur observatory for their help in observations and the maintenance of the antenna/receiver systems there. The details of the Hα observations in Kodaikanal observatory were provided by K. Prabhu. We acknowledge him. The referee's comments on the earlier version of the manuscript helped us to present the results more clearly. We thank him/her for that. The *SOHO* data are produced by a consortium of the Naval Research Laboratory (USA), Max-Planck-Institut fur Sonnensystemforschung (Germany), Laboratoire dAstronomie (France), and the University of Birmingham (UK). *SOHO* is a project of international cooperation between ESA and NASA. The *SOHO*/LASCO CME catalog is generated and maintained at the CDAW Data Center by NASA and the Catholic University of America in cooperation with the Naval Research Laboratory. The *SDO*/AIA data are courtesy of the NASA/*SDO* and the AIA science teams.

References

Bein, B., Berkebile-Stoiser, S., Veronig, A. M., et al. 2011, ApJ, 738, 191
Benz, A. O., Monstein, Ch., Meyer, H., et al. 2009, EM&P, 104, 277
Brueckner, G. E., Howard, R. A., Koomen, M. J., et al. 1995, SoPh, 162, 357
Cho, K.-S., Bong, S.-C., Kim, Y.-H., et al. 2008, A&A, 491, 873
Cho, K.-S., Gopalswamy, N., Kwon, R.-Y., Kim, R.-S., & Yashiro, S. 2013, ApJ, 765, 148
Cho, K.-S., Moon, Y.-J., Dryer, M., et al. 2005, JGR, 110, A12101
Clasen, H. T., & Aurass, H. 2002, A&A, 384, 1098
Cliver, E. W., Nitta, N. V., Thompson, B. J., & Zhang, J. 2004, SoPh, 225, 105
Cliver, E. W., Webb, D. F., & Howard, R. A. 1999, SoPh, 187, 89
Dulk, G. A., & McLean, D. J. 1978, SoPh, 57, 279
Dulk, G. A., & Suzuki, S. 1980, A&A, 88, 203
Ebenezer, E., Subramanian, K. R., Ramesh, R., SundaraRajan, M. S., & Kathiravan, C. 2007, BASI, 35, 111
Gopalswamy, N. 2006, in Solar Eruptions and Energetic Particles, ed. N. Gopalswamy, R. Mewaldt, & J. Torsti (Washington, DC: AGU), 207
Gopalswamy, N., Aguilar-Rodriguez, E., Yashiro, S., et al. 2005, JGR, 110, A12S07
Gopalswamy, N., Nitta, N., Akiyama, S., Mäkelä, P., & Yashiro, S. 2012, ApJ, 744, 72
Gopalswamy, N., Thompson, W. T., Davila, J. M., et al. 2009, SoPh, 259, 227
Gopalswamy, N., Xie, H., Akiyama, S., et al. 2013a, ApJL, 765, L30
Gopalswamy, N., Xie, H., Mäkelä, P., et al. 2013b, AdSpR, 51, 1981
Hariharan, K., Ramesh, R., & Kathiravan, C. 2015, SoPh, 290, 2479
Hariharan, K., Ramesh, R., Kishore, P., Kathiravan, C., & Gopalswamy, N. 2014, ApJ, 795, 14
Kathiravan, C., Ramesh, R., Indrajit, V. B., & Rajalingam, M. 2011, ApJ, 730, 2

Kishore, P., Kathiravan, C., Ramesh, R., Rajalingam, M., & Indrajit, V. B. 2014, SoPh, 289, 3995
Kishore, P., Ramesh, R., Hariharan, K., Kathiravan, C., & Gopalswamy, N. 2016, ApJ, 832, 59
Kishore, P., Ramesh, R., Kathiravan, C., & Rajalingam, M. 2015, SoPh, 290, 2409
Kumar, P., Innes, D. E., & Cho, K.-S. 2016, ApJ, 828, 28
Lemen, J. R., Title, A. M., Akin, D. J., et al. 2012, SoPh, 275, L17
Lin, J., Mancuso, S., & Vourlidas, A. 2006, ApJ, 649, 1110
Liu, W., & Ofman, L. 2014, SoPh, 289, 3233
Liu, Y., Luhmann, J. G., Bale, S. D., & Lin, R. P. 2009, ApJL, 691, L151
Ma, S., Raymond, J. C., Golub, L., et al. 2011, ApJ, 738, 160
Magdalenić, J., Marqué, Ch., Zhukov, A. N., Vršnak, B., & Veronig, A. 2012, ApJ, 746, 152
Mancuso, S., & Raymond, J. C. 2004, A&A, 413, 363
Mann, G., Klassen, A., Claßsen, H. T., et al. 1996, A&A, 119, 489
Mercier, C., Subramanian, P., Chambe, G., & Janardhan, P. 2015, A&A, 576, A136
Monstein, C., Ramesh, R., & Kathiravan, C. 2007, BASI, 35, 473
Mugundhan, V., Ramesh, R., Indrajit, V. B., et al. 2016, ApJ, 831, 154
Nindos, A., Aurass, H., Klein, K.-L., & Trottet, G. 2008, SoPh, 253, 3
Patsourakos, S., & Vourlidas, A. 2012, SoPh, 281, 187
Pohjolainen, S., Pomoell, J., & Vainio, R. 2008, A&A, 490, 357
Ramesh, R. 2011a, in Proc. Astron. Soc. India Conf. Ser. 2, 1st Asia-Pacific Solar Physics Meeting, ed. A. R. Choudhuri & D. Banerjee (Banglore: ASI), 55
Ramesh, R., Anna Lakshmi, M., Kathiravan, C., Gopalswamy, N., & Umapathy, S. 2012a, ApJ, 752, 107
Ramesh, R., Kathiravan, C., Indrajit, V. B., Beeharry, G. K., & Rajasekara, G. N. 2010a, ApJL, 719, L41
Ramesh, R., Kathiravan, C., Indrajit, V. B., & Rajalingam, M. 2012b, ApJ, 744, 165
Ramesh, R., Kathiravan, C., & Satya Narayanan, A. 2011b, ApJ, 734, 39
Ramesh, R., Kathiravan, C., Satya Narayanan, A., & Ebenezer, E. 2003, A&A, 400, 753
Ramesh, R., Kathiravan, C., Sreeja, S. K., & Gopalswamy, N. 2010b, ApJ, 712, 188
Ramesh, R., Kishore, P., Sargam, M. M., et al. 2013, ApJ, 778, 30
Ramesh, R., Nataraj, H. S., Kathiravan, C., & Sastry, Ch. V. 2006a, ApJ, 648, 707
Ramesh, R., & Sastry, Ch. V. 2000, A&A, 358, 749
Ramesh, R., Subramanian, K. R., & Sastry, Ch. V. 1999a, A&AS, 139, 179
Ramesh, R., Subramanian, K. R., & Sastry, Ch. V. 1999b, SoPh, 185, 77
Ramesh, R., Subramanian, K. R., Sundara Rajan, M. S., & Sastry, Ch. V. 1998, SoPh, 181, 439
Ramesh, R., Sundara Rajan, M. S., & Sastry, Ch. V. 2006b, ExA, 21, 31
Ravindra, B., Prabhu, K., Rangarajan, K. E., et al. 2016, RAA, 16, 127
Riddle, A. C. 1974, SoPh, 35, 153
Robinson, R. D. 1983, PASAu, 5, 208
Sasikumar Raja, K., Ingale, M., Ramesh, R., et al. 2016, JGRA, 121, 11605
SasikumarRaja, K., Kathiravan, C., Ramesh, R., Rajalingam, M., & Indrajit, V. B. 2013a, ApJS, 207, 2
Sasikumar Raja, K., & Ramesh, R. 2013b, ApJ, 775, 38
Shanmugaraju, A., Moon, Y.-J., & Vršnak, B. 2009, SoPh, 254, 297
Stewart, R. T., & McLean, D. J. 1982, PASAu, 4, 386
Temmer, M., Veronig, A. M., Kontar, E. P., Krucker, S., & Vršnak, B. 2010, ApJ, 712, 1410
Temmer, M., Veronig, A. M., Vršnak, B., et al. 2008, ApJL, 673, L95
Thompson, B. J., Plunkett, S. P., & Gurman, J. B. 1998, GeoRL, 25, 2465
Vršnak, B., & Cliver, E. W. 2008, SoPh, 253, 215
Vršnak, B., Magdalenić, J., Aurass, H., & Mann, G. 2002, A&A, 396, 673
Vršnak, B., Ruždjak, D., Zlobec, P., & Aurass, H. 1995, SoPh, 158, 331
Zhang, J., Dere, K. P., Howard, R. A., Kundu, M. R., & White, S. M. 2001, ApJ, 559, 452
Zimovets, I., Vilmer, N., Chian, A. C.-L., Sharykin, I., & Struminsky, A. 2012, A&A, 547, A6
Zucca, P., Pick, M., Démoulin, P., et al. 2014, ApJ, 795, 68